

# Extracellular *Streptomyces* vesicles: amphorae for survival and defence

Hildgund Schrempf,<sup>1\*</sup> Ilona Koebsch,<sup>1</sup>  
Stefan Walter,<sup>1</sup> Harald Engelhardt<sup>2</sup> and  
Holger Meschke<sup>1</sup>

<sup>1</sup>FB Biology/Chemistry, Applied Genetics of Microorganisms, University Osnabrück, Barbarastr. 13, D-49069 Osnabrück, Germany.

<sup>2</sup>Max Planck Institute of Biochemistry, Am Klopferspitz 18, D-82152 Martinsried, Germany.

## Summary

**Blue-pigmented exudates arise as droplets on sporulated lawns of *Streptomyces coelicolor* M110 grown on agar plates. Our electron microscopical and biochemical studies suggest that droplets contain densely packed vesicles with large assemblies of different protein types and/or the polyketide antibiotic actinorhodin. Frozen-hydrated vesicles were unilamellar with a typical bilayer membrane, and ranged from 80 to 400 nm in diameter with a preferred width of 150–300 nm. By means of cryo-electron tomography, three types were reconstructed three-dimensionally: vesicles that were filled with particulate material, likely protein assemblies, those that contained membrane-bound particles, and a vesicle that showed a higher contrast inside, but lacked particles. Our LC/MS analyses of generated tryptic peptides led to the identification of distinct proteins that carry often a predicted N-terminal signal peptide with a twin-arginine motif or lack a canonical signal sequence. The proteins are required for a range of processes: the acquisition of inorganic as well as organic phosphate, iron ions, and of distinct carbon sources, energy metabolism and redox balance, defence against oxidants and tellurites, the tailoring of actinorhodin, folding and assembly of proteins, establishment of turgor, and different signalling cascades. Our novel findings have immense implications for understanding new avenues of environmental biology of streptomycetes and for biotechnological applications.**

Received 6 January, 2011; accepted 12 January, 2011. \*For correspondence. E-mail schrempf@biologie.uni-osnabrueck.de; Tel. (+49) 541 969 28 95; Fax (+49) 541 969 28 04.

## Introduction

Streptomycetes are known to secrete an enormous repertoire of secondary metabolites, including antibiotics, antifungals and cytostatics, a broad spectrum of extracellular enzymes (i.e. agarases, chitinases, cellulases, proteases, lipases, phosphatases, xylanases) enzyme inhibitors as well as surface-anchored proteins (reviews: Schrempf, 2007; Chater *et al.*, 2010). *Streptomyces* genomes encode classical secretion systems for proteins that are known from other bacteria (review: Yuan *et al.*, 2010) including components for the Sec pathway. Based on the features of the signal peptide, proteins have been predicted, and in many cases proven, to be secreted via this system. A considerable number of *Streptomyces* proteins have been detected whose signal peptide comprises a consensus motif including invariant arginine residues (review: Chater *et al.*, 2010). These findings correlate with the experimental identification of the components for the Tat machinery (Schaerlaekens *et al.*, 2001).

Studies of non-classical protein-secretion mechanisms have been pursued dominantly within Gram-negative bacteria, and have culminated in characterizing six different specialized secretion systems, classified as types I–IV. An alternative secretion route for proteins, named type VII, has been identified in the Gram-positive *Mycobacterium tuberculosis*, and its genome encodes even five homologues (review: Abdallah *et al.*, 2007). Based on this knowledge, researchers investigated the biological role of a type VII system in *Streptomyces coelicolor* M145 (Akpe San Roman *et al.*, 2010).

Genes encoding proteins for the efflux of secondary metabolites of streptomycetes are usually located within the gene cluster for the corresponding biosynthesis. Many of these encode members of a multicomponent ABC transporter; this requires a ligand-binding protein, two permeases and a cooperating ATP-binding protein, and ATP hydrolysis as an energy source. Alternatively, a member of major facilitator superfamily (MFS comprising only one membrane protein) mediates the efflux of a small compound in response to chemiosmotic ion gradients (review: Martín *et al.*, 2005).

Depending on their chemical features, extracellular low-molecular-weight metabolites are either associated to the mycelium and/or distributed within the culture filtrate or agar plate. Coloured metabolites can be scored easily

visually; therefore, they have been evaluated in the course of traditional strain descriptions (Kutzner, 1981). Since more than 60 years several researchers have noticed that liquid exudates of various colours may arise on the top of elder sporulated colonies. These have been named 'colourless droplets of water' of *Streptomyces bikiniensis* (Johnstone and Waksman, 1947), 'exuded droplets' of *Streptomyces griseus* (Williams and McCoy, 1953), 'yellow guttation drops' of *Streptomyces scabies* (Bonde and McIntyre, 1968) and 'blue droplets' of *S. coelicolor* A3(2) (Rudd and Hopwood, 1979). Due to the pretty appearance, many researchers dealing with many different aspects of streptomycetes copy a colony with blue droplets to their web pages, slides for talks or on posters. Surprisingly, the detailed analyses of droplets have not been tackled.

In this report, we demonstrate for the first time that droplets of *S. coelicolor* M110, a derivative of *S. coelicolor* A3(2), comprise in addition to the coloured polyketide actinorhodin a huge battery of highly concentrated proteins, which occur within large assemblies. Interestingly, many of the identified proteins are different enzymes, or substrate-binding proteins. Investigations by electron microscopy and cryo-electron tomography led to the identification of robust vesicles, which are surrounded by distinct layer and have a highly structured interior. Taken together, the data reveal that the droplets contain vesicles, suggested to play roles in survival and defence.

## Results

### *General features of S. coelicolor M110 droplets*

M110 – a derivative of *S. coelicolor* A3(2) lacking the linear plasmid SCP1 – was inoculated with spores on plates containing agar with complete medium (see *Experimental procedures*). Following germination, substrate and aerial hyphae developed. Seven to 10 days later, droplets arose on top of the sporulated areas. The volume of visible droplets usually varied between 5 and 50  $\mu\text{l}$ ; their colour ranged between bright and darker blue (Fig. 1A).

The bottom of the droplets adhered tightly to the surface of sporulating colonies. Inspection by light microscopy (Fig. 1B) revealed that the base of the droplets was encased by hyphae. Upon simultaneous addition of DNA-intercalating dyes (SYTO9 and propidium iodine), living (green fluorescence) and dead (red fluorescence) hyphae appeared, and it became obvious that they attached external, rather than internal, to the droplets (Fig. 1C).

### *Droplets contain actinorhodin but not prodigiosin*

The droplets usually had a blue appearance (Fig. 1A), and they developed a red colour upon acidification. TLC

and LC/MS analyses, following extraction of acidified (pH 2–3) droplets with an equal mixture of chloroform and methanol, revealed that the red-coloured compound was not prodigiosin. Under alkaline conditions, the colour of the extract changed to dark blue. The absorption spectra showed typical characteristics of the polyketide antibiotic actinorhodin, which is blue under alkaline and red under acid conditions (see *Experimental procedures*).

### *Transmission electron microscopy shows the presence of vesicles*

Our investigations by transmission electron microscopy (TEM) revealed that droplets contain round and densely packed particles of different size (Fig. 2A). Larger vesicles (diameter 100–250 nm) and smaller particles with defined shapes (diameter 30–80 nm) were present (Fig. 2B and C). The abundance of non-stainable areas/surfaces on various vesicles was noticeable (Fig. 2C). The presence of vesicles, which had undergone different degrees of disruption, was attributed to their fragility during the process of preparation and negative staining.

Fractions that had been obtained after subjecting droplets to flotation in a sucrose gradient (see one following chapter) still comprised vesicles; however, due to dilution and possible damage during this process, they were less abundant (Fig. 2D).

### *The identified proteins play roles in survival and defence*

Droplets contained large quantities of protein (ranging from 1 to 2  $\mu\text{g } \mu\text{l}^{-1}$ ). After separation of proteins by electrophoresis (Fig. 3A, lanes 1–2) and in-gel digestion with trypsin, we analysed the resulting peptides by LC/MS (Aebersold and Mann, 2003). Subsequently, we made investigations for originating proteins, possible domain(s) and signal peptides as well as the corresponding genes, which were derived from individual studies and/or from genomic sequence data (Table 1). In many cases, trypsin had cleaved the separated proteins to a large number of identifiable fragments. Thus, MS/MS scores ranged from 1500 to 500 and 499 to 150. Only in a few cases, i.e. less abundant smaller proteins, the scores were lower (149 to 79, with three or more assigned peptides). Proteins, which had been identified on the basis of the generated fragments, were only considered, if they also matched to the apparent molecular weight within the gel. The experiments were repeated several times, and only those proteins have been listed that were found consistently.

A remarkable number of the detected proteins carry an N-terminal signal peptide with a twin-arginine motif (i.e.

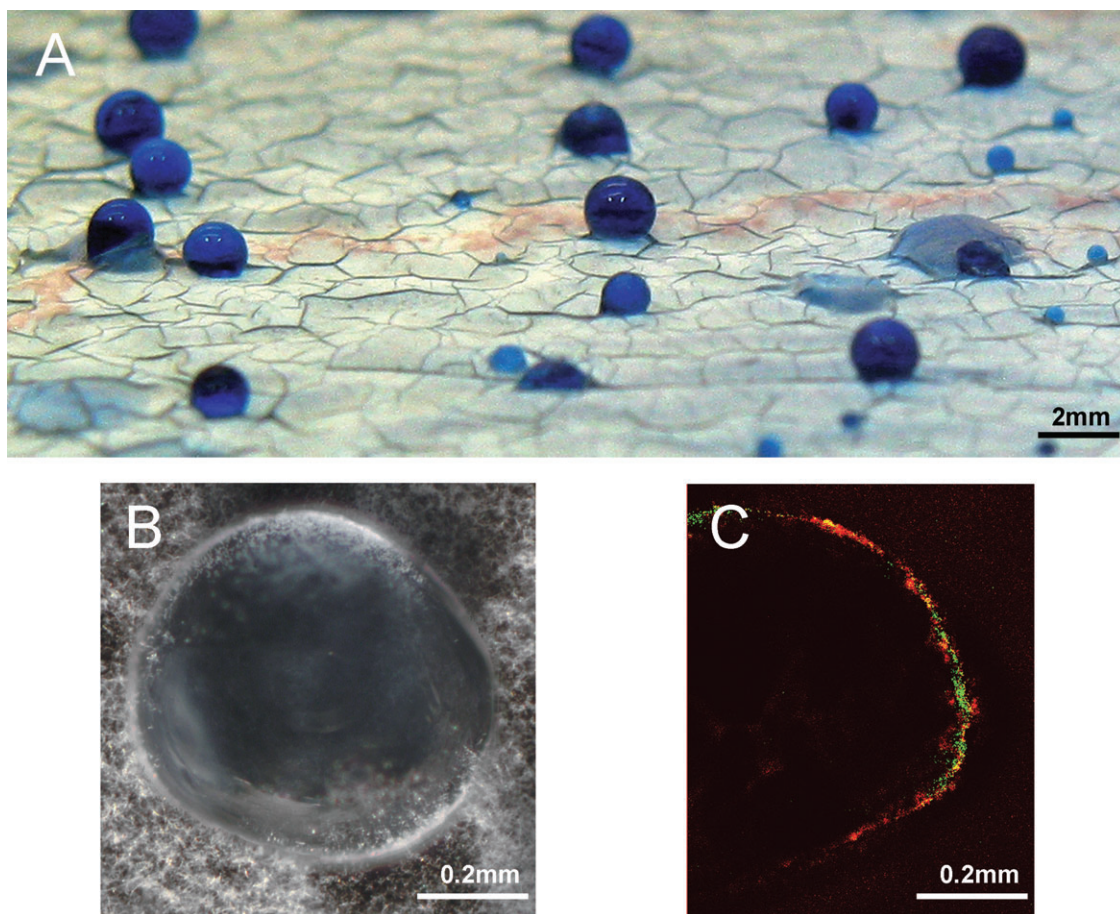


**Fig. 1.** Macroscopic and microscopic presentations of droplets. Blue droplets on an agar plate were inspected directly. A. A photograph (use of a macro lens) of blue droplets arising on top of the sporulating *S. coelicolor* M110 is presented. B. A small drop has been inspected by light microscopy (40 $\times$ ) and photographed. Aerial mycelium (white) is surrounding the blue droplet. C. The dyes SYTO9 and propidium iodine were added applied simultaneously with a needle into the drop. A serial of images was taken with a confocal microscope (see *Experimental procedures*). A superimposed image is presented. The outside rim of the droplet consists of hyphae with a red, green or merged fluorescence. The inside of the droplet has only some marginal background fluorescence and lacks hyphae.

SCO No.: 1230, 1565, 1639, 3471, 3484, 4142, 5074, 6065, 6281 and 6691). The genes for these proteins are spread over a large area of the genome, and none of them resides close to each other. All these proteins are either predicted enzymes or ligand-binding proteins. Additionally, one enzyme (SCO1639) and the ligand-binding proteins (SCO3484 and SCO6065) contain a potential lipid attachment site. However, another binding protein has a predicted Sec transit peptide (SCO4142) in contrast to the corresponding homologue from *Streptomyces lividans* (Table 1), which possesses a predicted Tat signal peptide. Interestingly, the peptides that we have identified experimentally have a closer relationship to the *S. lividans* counterpart (see *Discussion*). The enzyme SCO1968 has a predicted Sec signal peptide. The other proteins lack any classical signal peptide (Table 1). The corresponding genes for the detected proteins are also situated apart

from each other, although some of them are situated relatively close to one chromosomal end (SCO No.: 0379, 0641, 0852, 0999, 1169, 2113, 2180, 2368, 2633, 2770 and 3767).

The identified proteins are predicted to be important for a range of processes: the acquisition of inorganic as well as organic phosphate, iron ions, and of distinct carbon sources, energy metabolism and redox balance, SOS response, defence against oxidants and tellurites, the tailoring of actinorhodin, folding and assembly of proteins, establishment of turgor, and different signalling cascades (Table 2 and discussion).

We have encountered neither ribosomal proteins nor elongation factors (i.e. EFTu or EFG), which are the most abundant cellular proteins. Therefore, we conclude that proteins in droplets (Table 1) have not emerged as a result of cell lysis.

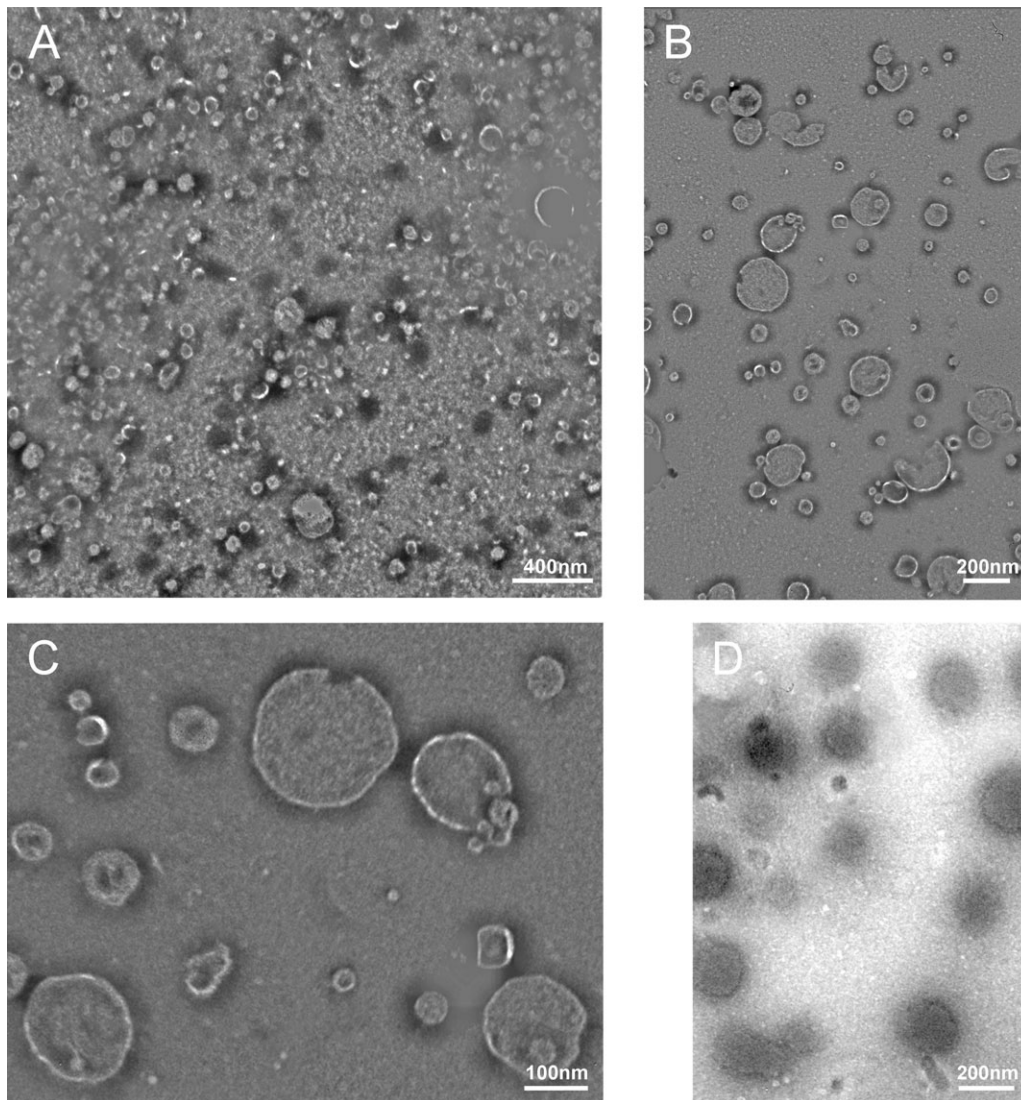


**Fig. 2.** Analyses of droplet samples by transmission electron microscopy (TEM). Samples of droplets were prepared on grids using standard methods as outlined under *Experimental procedures*, and inspected by TEM.

A. An overview is presented.

B and C. At higher magnifications, individual vesicles of different sizes are detected.

D. A blue droplet had been subjected to centrifugation in a sucrose gradient (floatation). A fraction (containing 30% sucrose) has been analysed by TEM using the Zeiss EM 902A microscope.

#### *Proteins and actinorhodin appear in different high-molecular-weight assemblies*

Portions of droplets were analysed (SDS-PAGE) for the presence of proteins either directly (control, Fig. 3B, lane 1) or after centrifugation in a sucrose gradient. The studies showed that proteins co-migrated during sedimentation (Fig. 3B, lanes 2–4) or floatation (not shown). All protein-containing fractions contained in addition actinorhodin and retained vesicles, which we detected by TEM (Fig. 2D).

Arrays corresponding to high-molecular-weight complexes were detected within droplets by gel filtration

(Sephacryl S-300, Fig. 3C). The protein analyses (SDS-PAGE) indicated the abundance of different mixtures (Fig. 3C, lanes 2–3; lanes 4–5). Based on these results and those described above, we concluded that the droplets contain various types of vesicles with different protein assemblies and/or actinorhodin.

#### *Three-dimensional reconstruction of vesicles by cryo-electron tomography*

To minimize damaging effects by standard TEM (see above), samples of droplets were embedded in vitreous ice (see *Experimental procedures*) and subjected to cryo-

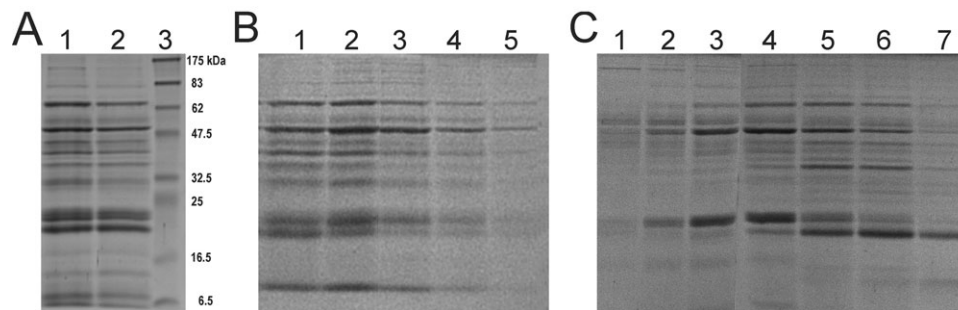


**Fig. 3.** Analyses of proteins and their assemblies. Proteins within the samples were separated by SDS-PAGE, stained and photographed. A. An aliquot (7  $\mu$ l) from two individual droplets (lanes 1 and 2) and a protein standard (lane 3) were investigated. B. An aliquot of a droplet (35  $\mu$ l) was subjected to centrifugation in a sucrose gradient (5–30%, sedimentation). The control (7  $\mu$ l prior centrifugation, lane 1) and an aliquot (35  $\mu$ l) of fractions, which have been collected after centrifugation at 15% (lane 2), 17.5% (lane 3), 20% (lane 4) or 22.5% (lane 5) sucrose, are presented after SDS-PAGE. C. An aliquot (100  $\mu$ l) of a droplet was subjected to gel filtration (Sephacryl-S300). Aliquots (30  $\mu$ l) of consecutively eluted fractions (lanes 1–7) are presented after SDS-PAGE. Controls are in (A), lanes 1 and 2.

electron microscopy. The dominant structural constituents in the droplets were verified to be vesicles (Fig. 4). The majority had a diameter between 80 and 400 nm in projection, with a preferred width of 150–300 nm. Since we cannot exclude flattening due to limited ice thickness, the upper diameter might be < 400 nm. The vesicles are unilamellar throughout with only one exception detected (not shown), which accounts for  $\approx$  1% of the inspected vesicles. The vesicle membrane exhibits the characteristic structure of lipid bilayers that is expected to be consistent with the imaging conditions used (Hoffmann *et al.*, 2008). We found three major categories of vesicles: apparently ‘empty’ ones that contained no detectable biological material inside or

associated with the membrane (Fig. 4A), vesicles that were scarcely or moderately filled with soluble material and showed a layer of densely packed particles associated to the outer and/or inner surface of the membrane (Fig. 4B–G), and vesicles that were heavily filled with putative protein complexes in aggregated form (Fig. 4H and I). The second and third type accounted for about 80–90% of the vesicles, and due to the gentle sample preparation, we observed few broken types.

Since low-dose projections of cryo-preparations do not allow the visualization of structural details at sufficient signal-to-noise ratio, we reconstructed characteristic vesicles three-dimensionally by means of cryo-electron

**Table 1.** List of identified proteins.

SCO No.	MW	Deduced function	Remarks			
			N	T	S	L
6691	75.667	Phospholipase C		T		
1230	58.499	Tripeptidyl aminopeptidase		T		
6281	58.486	Oxidoreductase (FAD binding)		T		
0379	55.082	Catalase	N			
2180	51.365	Dihydrolipoamide dehydrogenase	N			
3484	46.229	Glycerol-3-phosphate-binding protein		T		L
1169	42.979	Xylose isomerase	N			
1565	42.649	Glycerophosphoryl-phosphodiesterase		T		
4142	38.107	Phosphate-binding protein		T <sup>Sl</sup>	S <sup>Sc</sup>	
3471	35.142	Agarase		T		
1639	34.915	Peptidyl-prolyl <i>cis-trans</i> -isomerase		T		L
2770	34.281	Agmatinase	N			
6065	33.661	Glycine-betaine-proline-binding protein		T		L
1968	31.400	Phospholipase C-like			S	
5074	23.120	Dehydratase		T		
0999	23.585	Fe/Mn superoxide dismutase	N			
2633	23.382	Fe/Mn superoxide dismutase	N			
0852	21.087	Aldolase-KHG type	N			
2368	20.378	TerD-like	N			
0641	20.168	TerD-like	N			
2113	19.208	Bacterio-ferritin-like protein	N			
3767	16.595	TerB-like	N			

N, no predicted signal peptide; S, predicted Sec signal peptide; T, predicted Tat signal peptide; L, predicted lipoprotein.

**Table 2.** Classification of proteins.

Class	Function	Protein	Additional role
Phosphate metabolism	Binding of P <sub>i</sub> Release of P <sub>o</sub>	Phosphate-binding protein	
		Glycerophosphoryl-phosphodiesterase	
		Phospholipase C	Signalling
		Phospholipase C-like	Signalling
Iron metabolism	Storage	Bacterio-ferritin-like protein	Antioxidant
Amino acids and derivatives	Binding Generation of metabolites	Glycine-betaine-proline-binding protein	Turgor
		Agmatinase	Signalling
Proteins	Cleavage Folding	Tripeptidyl aminopeptidase	
		Peptidyl-prolyl <i>cis</i> - <i>trans</i> -isomerase	Assembly
Carbon utilization	Hydrolysis Metabolic pathways	Agarase	
		Glycerol-3-P-binding protein	
		Xylose isomerase	
		KHG aldolase	SOS response
		Dihydrolipoamide dehydrogenase	Pro-oxidant
Reactive oxygen species	Antioxidants	Superoxide dismutases	
		Catalase	Tellurite defence?
Tellurite	Resistance	TerD-like proteins TerB	Signalling
Polyketide	Tailoring modification	Dehydratase Oxidoreductase (FAD)	

tomography. In addition to the membrane bilayer, the apparently empty vesicles did not show any detectable densities in tomograms (data not shown). The reconstruction (Fig. 5) shows vesicles with putatively membrane-bound particles (about 3–8 nm in size) inside and outside the membrane, and a vesicle (V3, Fig. 5F) whose lumen is densely packed with macromolecular material that tends to form various aggregates. While vesicle V1 is apparently free of heavily aggregated complexes, V2 (Fig. 5F) exhibits a higher but homogeneous electron density. To evaluate whether these differences are meaningful, we compared the statistics and density distributions of voxels extracted from the lumina of reconstructed vesicles V1, V2, V3 and from the background (Table 3). All the density distributions are significantly different from each other according to Chi-square tests for homogeneity ( $P \ll 0.001$ ). Vesicle V3 showed the lowest mean value of voxels and, thus, contained the highest mass inside. Since the mean value of V1 was smaller than the background value, it is expected to contain some mass other than ice in addition. Vesicle V2 was homogeneously filled with molecules of low molecular weight (less granularity than in V3, also indicated by a smaller SD value) that could not be resolved in our reconstruction. We conclude that the membrane vesicles vary in their structure, macromolecular composition, both membrane-associated and soluble material.

## Discussion

We have discovered densely packed small (diameter 30–80 nm) and larger (diameter 100–250 nm) vesicles within the extracellular droplets (Fig. 2) of *S. coelicolor*

M110 using standard fixation techniques and TEM. In frozen-hydrated samples, we observed even larger vesicles (diameter 80–400 nm) and identified the typical bilayered structure of lipid membranes (Figs 4 and 5). Our findings show for the first time the presence of extracellular vesicles in a Gram-positive *Streptomyces* strain. Up to now, knowledge of extracellular vesicles in Gram-positive bacteria is very limited. Only recently, other authors have detected by TEM outer membrane vesicles (diameter 20–100 nm) within highly concentrated culture filtrates of *Staphylococcus aureus* (Lee *et al.*, 2009). In contrast, different researchers have enriched varieties of outer membrane vesicles (20–200 nm) from culture filtrates of a range of Gram-negative bacteria (review: Kulp and Kuehn, 2010).

Previously reported techniques for the isolation of natural outer membrane vesicles include removal of bacterial cells by centrifugation, high-speed centrifugation of the cleared culture filtrate, and suspension of the resulting pellet, which contains cell debris, proteins and vesicles. Subsequent sedimentation and (or) flotation in gradients is then necessary to enrich the vesicles. One litre of culture filtrate contained only small quantities of vesicles (200 µg wet weight) from *S. aureus* (Lee *et al.*, 2009), or, respectively, vesicle proteins (30 µg) from *Xanthomonas campestris* (Sidhu *et al.*, 2008). In contrast, the vesicle-containing droplets of *S. coelicolor* M110 are extremely protein-rich (1–2 µg µl<sup>-1</sup>). After centrifugation of the droplets in a sucrose gradient the total amount of proteins remains almost unchanged, with only their concentration being diluted up to fivefold by the process.

The *S. coelicolor* M110 vesicle-containing droplets comprise repertoires of proteins that are useful for survival

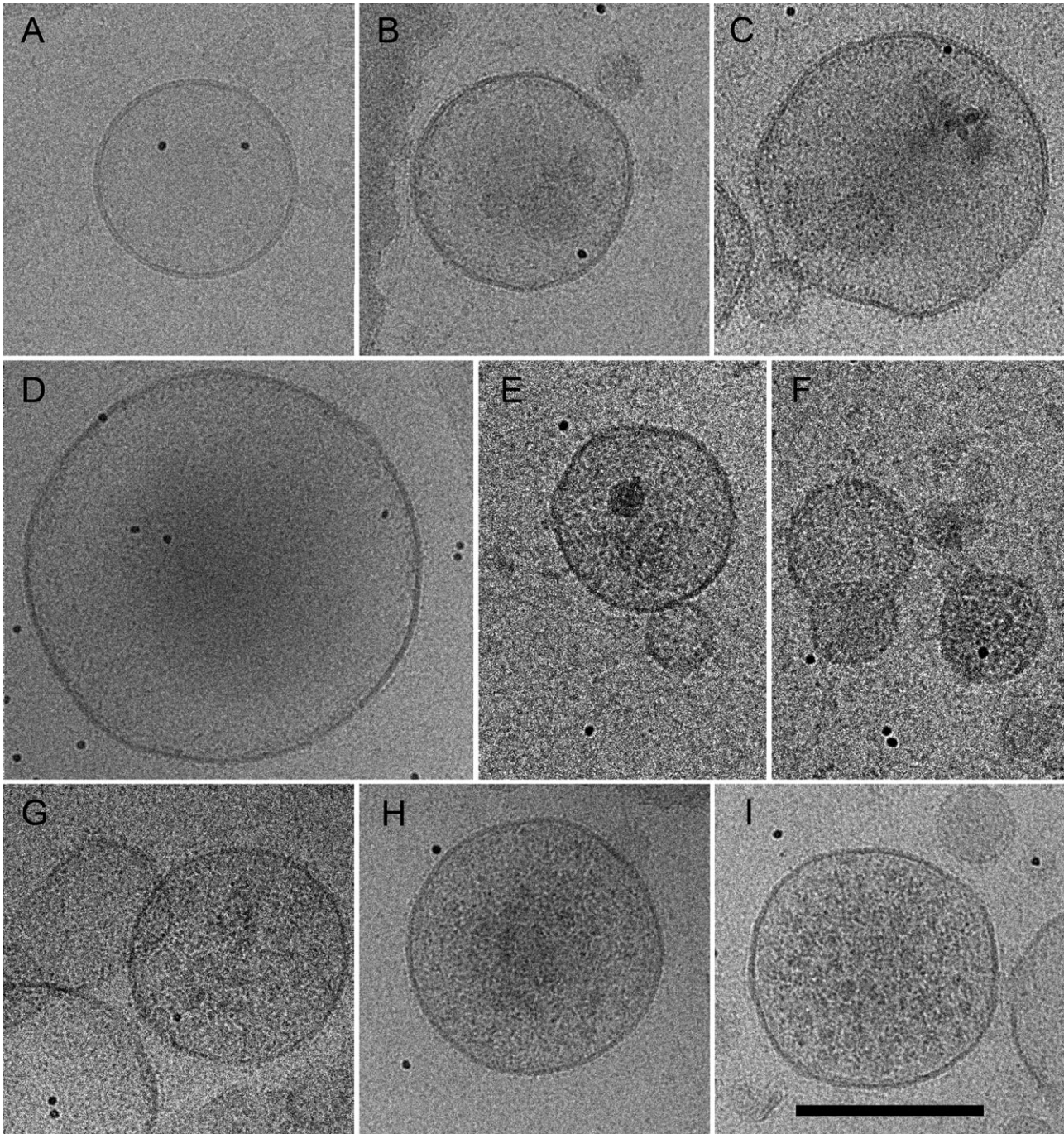


**Fig. 4.** Investigations of droplets by cryo-electron microscopy. Frozen-hydrated samples of droplets were analysed by cryo-electron microscopy. Different types of vesicles were identified: (A) apparently empty vesicles, (B–G) empty or moderately filled vesicles with membrane-associated or membrane-bound protein complexes in outside and inside orientation, (H and I) vesicles heavily filled with material (see also vesicle on the right in F and in Fig. 5). The black dots originate from gold markers (10 nm), which had been added to the sample. The scale bar represents 200 nm and is valid for all images.

and defence (see below). Remarkably, they lack components for protein biosynthesis (i.e. ribosomal proteins, elongation factors, tRNA synthetases), transcription (i.e. subunits of DNA-dependent RNA polymerase), glycolysis (i.e. glyceraldehyde-3-phosphate-dehydrogenase, pyru-

vate kinase), and several other cytoplasmic enzymes that have been found within vesicle preparations of *S. aureus* (Lee *et al.*, 2009). These proteins are present in high quantities in living cells; this might allow the interpretation that they are contaminants of cell debris of *S. aureus*.

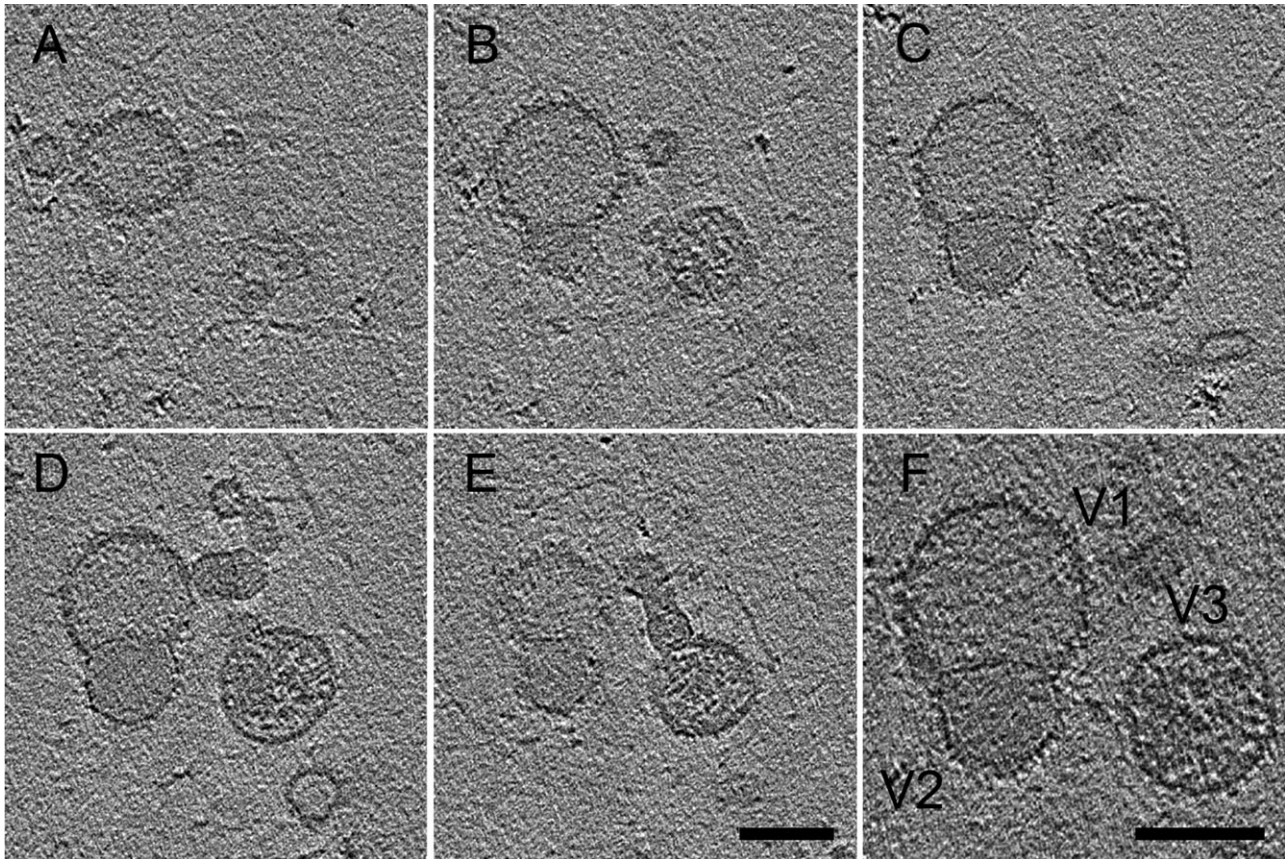


**Fig. 5.** Three-dimensional reconstruction of vesicles by cryo-electron tomography.

A–E. Slices ( $xy$ ) through the reconstructed three-dimensional volume of vesicles (original projection image: see Fig. 4F) are presented. The distance in  $z$ -direction between consecutive slices is 25.8 nm with a voxel size in  $z$  of 0.55 nm.

F. The slice situated at  $z$ -position in subfigure C was averaged over 1.7 nm to reduce noise and enhance contrast. Vesicles V1 and V2 are attached and show apparently membrane-bound particles at the outer surface. V3 is densely filled with material, presumably protein complexes in variously aggregated states. Vesicle V2 does not show particles in its lumen but exhibits a higher contrast than V1. This indicates accumulation and homogeneous distribution of soluble molecules that are not structurally resolved.

Bars represent 100 nm.

However, our studies by confocal and electron microscopy (Figs 1C and 2) revealed that the interior of the droplets was free of *Streptomyces* hyphae. This makes the *S. coelicolor* M110 droplets a thus far unique source for highly concentrated vesicles.

The proteins within the vesicle-comprising droplets will be discussed in the following paragraphs according to their functional context. The detected phosphate-binding protein PtsS of *S. coelicolor* M110 relates slightly more

**Table 3.** Density statistics from subvolumes of reconstructed vesicles.

Subvolume	Number of data	Density value of voxels (mean $\pm$ SD)
Background (ice)	203 339	127.0 $\pm$ 35.0
Lumen of vesicle 1	125 378	124.7 $\pm$ 36.4
Lumen of vesicle 2	47 047	119.2 $\pm$ 34.2
Lumen of vesicle 3	93 738	117.3 $\pm$ 43.0

closely to one described *S. lividans* PtsS protein including a Tat signal peptide, rather than to the expected *S. coelicolor* SCO4142 protein with a Sec signal peptide. The *S. lividans* PtsS has a predicted lipid attachment site; however, under a range of conditions it accumulates in the culture filtrate (Díaz *et al.*, 2005). Bacteria usually capture the essential phosphate in inorganic form using specific ABC transporters comprising the above-mentioned type of phosphate-binding protein. In a natural environment, bacteria frequently encounter a scarcity of inorganic phosphate. To compensate, they frequently utilize a range of organic phosphorous compounds. The secreted proteins SCO1565 and SCO1968 from *S. coelicolor* M110 have a glycerophosphodiester phosphodiesterase domain; this is known to hydrolyse glycerophosphodiesters (derived by deacetylation of phospholipids) to glycerol-3-phosphate and the corresponding alcohol moiety. Previous studies (Santos-Beneit *et al.*, 2009) showed that the presence of inorganic phosphate inhibited the expression of both the

genes encoding SCO1565 and SCO1968. One encountered *S. coelicolor* M110 protein SCO3484 is related to an *Escherichia coli* protein, which is required for binding glycerol-3-phosphate. In contrast to *E. coli*, the *S. coelicolor* M110 counterpart is predicted to be lipid-anchored. Our data show that the *S. coelicolor* M110 vesicle-containing droplets are well equipped to deal with phosphate scarcity.

The detected *S. coelicolor* M110 proteins SCO6691 and SCO1968 correspond to a phosphocholine-specific phospholipase C (Stonehouse *et al.*, 2002), and, respectively, to a member of a phosphoinositide-specific phospholipase C-like type. In recent years, phosphatidylcholine preferring phospholipases C (PC-PLC) have been associated with a growing number of signal transduction mechanisms in eukaryotic cells. The PI-PLC-like phosphodiesterases superfamily includes also the catalytic domains of bacterial phosphatidylinositol-specific phospholipase C types. These enzymes generate inositol 1, 4, 5 triphosphate, a universal calcium-mobilizing second messenger and diacylglycerol, known as an activator of certain protein kinases in eukaryotes (Katan, 2005).

*Streptomyces coelicolor* A3(2) utilizes agar as a carbon source, because the strain secretes an agarase in a Tat-dependent fashion (review: Chater *et al.*, 2010); this enzyme is also present in the *S. coelicolor* M110 droplet-containing vesicles. D-xylose is a common carbon source in nature. The identified xylose isomerase SCO1169 corresponds to an abundant microbial enzyme that catalyses the reversible isomerization of D-xylose to D-xylulose, and also accepts D-glucose and D-fructose as substrates (Heo *et al.*, 2008). KHG (2-keto-4-hydroxyglutarate aldolase, also called 2-keto-3-deoxy-6-phosphogluconate aldolase) is a multifunctional enzyme that is involved in the glyoxylate and the Entner–Doudoroff pathway. For the recovery following SOS response, *E. coli* requires KHG (Cayrol *et al.*, 1995). It is remarkable that the vesicle-containing droplets of *S. coelicolor* M110 are equipped with this versatile enzyme type, SCO0852 (Tables 1 and 2).

The cell turgor within microorganisms is adjusted by controlling the pool of osmolytes, so-called compatible solutes, including among others proline, betaine and ectoine. In addition, these solutes serve as stabilizers of proteins against denaturing effect of high ionic strength (review: Kempf and Bremer, 1998). The occurrence of a lipid-anchored binding protein SCO6065 for proline, betaine and ectoine suggests that these solutes may exhibit the above-outlined dual function in *S. coelicolor* M110 vesicles. Arginine derives from proline or glutamate, and is the precursor for several cellular metabolites including polyamines, nitroxide (NO) and agmatine. The synthesis of NOs and polyamines depends on agmatine, which has been shown to be a competitive inhibitor of NO

synthase (Grillo and Colombatto, 2004). Based on this knowledge, we expect the *S. coelicolor* M110 agmatinase (SCO2770) to play a corresponding role and, therefore, to affect also the level of NO that researchers recognize increasingly as signalling molecule (Nathan, 2004).

Another predicted enzyme with a Tat signal peptide (SCO1230) is a homologue of the tripeptidyl aminopeptidase, previously isolated as extracellular enzyme from *S. lividans*, it removes tripeptides from an unmodified N-terminus of small proteins and polypeptides (Butler *et al.*, 1995). Interestingly, a *Pseudomonas aeruginosa* aminopeptidase was found both externally and associated with outer membrane vesicles. Other authors have reported that murein hydrolase of a *P. aeruginosa* strain can reside in membrane vesicles (Li *et al.*, 1996) which in addition may contain quinolone molecules with antimicrobial activity (review: Mashburn-Warren and Whiteley, 2006).

In addition to the diversity of proteins, we found the polyketide antibiotic actinorhodin in the vesicle-containing droplets of *S. coelicolor* M110. Interestingly, we also identified a protein with a predicted Tat signal peptide that is required as dehydratase (ActVI-ORF3, SCO5074) for one of the late actinorhodin-tailoring steps. This enzyme had previously been found by a proteomic approach within the culture supernatant of the strain M600, a derivative of *S. coelicolor* A3(2) (review: Chater *et al.*, 2010). Notably, we also detected the oxidoreductase SCO6281 with a FAD-binding and a BBE domain (corresponding to the berberine bridge enzyme), and a predicted Tat signal peptide among the vesicle proteins of *S. coelicolor* M110. Enzymes carrying these domains are flavinylated oxygen oxidoreductases for specific substrates. Self-resistance against mitomycin C in *Streptomyces lavendulae* is mediated by a member of this enzyme family, which has been proposed to mediate oxidation of this antitumour antibiotic (August *et al.*, 1994). It will be interesting to identify the substrate of the SCO6281 protein.

Harmful compounds include hydrogen peroxide (H<sub>2</sub>O<sub>2</sub>) and reactive oxygen species. H<sub>2</sub>O<sub>2</sub> is produced in the environment by chemical processes and by photochemical mechanisms; it is an uncharged molecule known to freely cross membranes and, hence, enter cells (review: Imlay, 2008). Reactive oxygen species could react with components of vesicles and, thus, induce damaging effects. The identified superoxide dismutases from *S. coelicolor* M110 belong to members of the FeSOD/MnSOD family; these are first-line antioxidant proteins, as they catalyse the dismutation of superoxide into oxygen and hydrogen peroxide. Typically, these enzymes lack a signal peptide, and usually reside either within the cytoplasm or within periplasmic space of various bacteria. However, *S. coelicolor* M110 has two identified extracellular SODs (SCO0999 and SCO2633, Table 1) within the

vesicle-containing droplets. So far, it was known that *M. tuberculosis* secretes FeSOD by an unknown mechanism within macrophages (Bendtsen *et al.*, 2004). The identified catalase of *S. coelicolor* M110 also lacks a signal peptide (SCO0379, Table 1); similarly, the catalase KatA from *Bacillus subtilis* has been recognized as non-classically secreted protein (Bendtsen *et al.*, 2005). Catalases accelerate the rate of the dismutation of H<sub>2</sub>O<sub>2</sub> (including that one generated by SODs) to molecular oxygen and water.

The identified *S. coelicolor* M110 bacterio-ferritin-like protein SCO2113 belongs to the ferritin superfamily. Members of these proteins are involved to store iron in their ferric form and/or in their detoxification or the protection against O<sub>2</sub> and its radical (review: Carrondo, 2003).

Oxidative cellular damage by the highly toxic potassium tellurite (KTeO<sub>3</sub><sup>2-</sup>) is in part due to the generation of the reactive oxygen species, superoxide radicals. Studies of *Pseudomonas pseudoalcaligenes* KF707 showed that levels of the classical antioxidant enzymes (i.e. superoxide dismutase and catalase) were increased after exposure to KTeO<sub>3</sub><sup>2-</sup>. Many catalases also bind the cofactors NADPH and NADH tightly, but, surprisingly, NAD(P)H is not required for their dismutase activity. However, a subset of both bacterial and mammalian catalases catalyse the NAD(P)H-dependent reduction of the highly toxic tellurite TeO<sub>3</sub><sup>2-</sup> to the less toxic elemental Te<sup>0</sup> *in vitro* (Calderón *et al.*, 2006). Possibly, the identified *S. coelicolor* M110 catalase has such an accessory role and, therefore, might act in concert with the additional defence repertoire against toxic tellurites (see below).

Several tellurite resistance genes have been identified, but their functions are unknown. We identified *S. coelicolor* M110 homologues of the proteins TerD and TerB. The *Klebsiella pneumoniae* TerD is known as tellurite-resistance protein (20.5 kDa) of unknown function, and its three-dimensional structure has been elucidated. Additional studies revealed that TerD binds Ca<sup>2+</sup>, and a novel bipartite Ca<sup>2+</sup>-binding motif has been defined that is predicted to be highly conserved in TerD proteins. Interestingly, these Ca<sup>2+</sup> binding sites also reside within two additional tellurite resistance proteins, TerE and TerZ. These results have led to the suggestion that Ca<sup>2+</sup> could play a crucial role in responses of bacteria to multiple external stimuli that depend on these Ter proteins (Pan *et al.*, 2011). The NMR structure of TerB – an additional *K. pneumoniae* Ter protein – is so far unique (Chiang *et al.*, 2008). As the found *S. coelicolor* M110 TerD and TerB belong to highly abundant proteins within the vesicle-containing droplets, an elucidation of their functional role will be rewarding.

It is an emerging view that bacteria seem to cope with TeO<sub>3</sub><sup>2-</sup> by general adaptation mechanisms. Recently, *Aeromonas caviae* ST was found to have a complex (compo-

nents E1, E2 and E3) to reduce K<sub>2</sub>TeO<sub>3</sub> in a NADH-dependent reaction. Interestingly, the tellurite reductase activity relies almost exclusively on the E3 component corresponding to dihydrolipoamide dehydrogenase (DLD). *In vitro* studies showed that this activity is also present within several other bacteria including *E. coli*, *Zymomonas mobilis*, *Streptococcus pneumoniae* and *Geobacillus stearothermophilus* (Castro *et al.*, 2008). It is interesting that we also found DLD (SCO2180 without a predicted signal peptide) within the *S. coelicolor* M110 vesicle-containing droplets. The enzyme DLD is usually an intracellular flavin-dependent oxidoreductase, which cooperates with certain multienzyme complexes as it utilizes dihydrolipoic acid and NAD<sup>+</sup> to reversibly generate lipoic acid and NADPH. In addition, DLD is able to catalyse the oxidation of NADH to NAD<sup>+</sup> by using different electron acceptors including O<sub>2</sub> and labile ferrous irons. In this capacity, DLD is believed to have a pro-oxidant role, which is achieved by reduction of O<sub>2</sub> to a superoxide radical or ferrous iron, which in turn catalyses the production of hydroxyl radical via the Fenton reaction. DLD can also scavenge nitric oxide and reduce ubiquinone to ubiquinol. Therefore, DLD is a versatile oxidoreductase with multiple roles in energy metabolism and redox balance.

One *S. coelicolor* M110 protein (SCO1639) belongs to the group of FK506-binding proteins, members of peptidyl-prolyl *cis/trans*-isomerases; these catalyse the *cis/trans*-isomerization between native-state prolyl bond isomers, and promote protein folding and assembly of multiprotein complexes *in vitro*. The physiological functions are poorly understood; researchers suggest possible roles in protein translation, folding, assembly and trafficking (Golbik *et al.*, 2005).

Based on the gel filtration studies (Fig. 3C), we concluded that distinct vesicles vary in their protein pattern. Therefore, vesicles were analysed by additional methods. After vitrification of natural samples that were directly obtained from droplets, investigations by cryo-electron microscopy and three-dimensional reconstruction revealed a considerable heterogeneity of vesicles, but also some remarkable structural features (Figs 4 and 5) that are not preserved in negative stain preparations (Fig. 2). Many vesicles are covered by membrane-associated or -bound proteins on the outer surface. It is currently unclear whether they (only) stabilize the vesicle membrane or represent functional enzyme complexes that are actively deposited in the vesicles membranes or that are required for transport. To date, it is still a challenge to investigate membrane proteins by means of cryo-electron tomography (Hoffmann *et al.*, 2008; Niederweis *et al.*, 2010). The majority of vesicles contained particulate material in the lumen in various amounts. Again, we cannot currently judge whether these are distinct complexes or mixtures of proteins. But it is tempting to specu-

late that aggregates preferably consist of one protein type that may form ordered or even microcrystalline particles. Future investigations with tomograms at higher resolution and probing the structure of protein complexes by the template matching approach (Frangakis *et al.*, 2002), using high-resolution structures of proteins occurring in vesicles, will give clues as to the identity and composition of proteins in individual vesicles. An interesting result is that apparently 'empty' vesicles, i.e. those without a clear particulate interior, are filled with some material, increasing the average electron density in tomograms. It will be a challenge to unravel the identity of this likely low-molecular compound(s); one possible candidate is the antibiotic actinorhodin.

The molecular mechanisms leading to the release of vesicles from Gram-negative bacteria are still not well understood. Based on the limited knowledge, researchers have concluded that the generation of outer membrane vesicles involves several steps: localized reductions of contacts between the outer membrane, proteins and peptidoglycan, effects on localized membrane curvature, as well as local changes in the distribution of particular proteins (review: Kulp and Kuehn, 2010). Our ongoing studies have indicated that in addition to *S. coelicolor* M110, other *Streptomyces* strains release vesicles. As the cell wall architecture of these Gram-positives differs from that of Gram-negative bacteria, streptomycetes will be promising candidates to elucidate selected aspects of vesicle biogenesis. In this context it will be also rewarding to explore the sorting process of proteins into the vesicles. The *S. coelicolor* M110 proteins with a Tat signal peptide motif are expected to transverse the membrane. Interestingly, the ligand-binding proteins have a predicted Tat signal peptide and a lipid attachment site; hence, their association with the vesicle membrane is likely (Table 1).

A large proportion of the proteins from *S. coelicolor* M110 vesicles lack a classical secretion signal, and are not predicted to be secreted according to software analyses by SecretomeP, which is an appropriate tool for identifying non-classical and leaderless protein secretion (Bendtsen *et al.*, 2005). Despite the extensive knowledge accumulated for Gram-negative bacteria, recent studies indicate that many aspects of secretion and targeting of bacterial proteins are still poorly understood. The study of secretion machineries (i.e. type I, II, IV) of Gram-negative bacteria suggests that several motifs within a protein can form a conformational signal for targeting. In another case (type IV), targeting of a specific protein requires the cooperation with a chaperone (Filloux, 2010). The shedding of outer membrane vesicles in Gram-negatives appears to be independent of known secretion systems.

Certain Gram-negative bacteria (i.e. *Helicobacter pylori*, cytotoxin-producing *E. coli*, *Shigella dysenteriae*) deliver their specific toxins within membrane vesicles to a

eukaryotic target cell (Kuehn and Kesty, 2005). Trafficking of a  $\beta$ -lactamase within membrane vesicles among a population of *P. aeruginosa* is a good example of sharing a gene product without the neighbouring cells containing the corresponding gene. In future, it will be interesting to test whether *Streptomyces* vesicles play a role in the delivery of proteins and small molecules during the interaction among streptomycetes as well as with other organisms. Additional knowledge on *Streptomyces* vesicles is also expected to ultimately provoke a range of biotechnological applications.

## Experimental procedures

### Strain and cultivation

*Streptomyces coelicolor* M110 is a derivative of *S. coelicolor* A3(2), which lacks the linear plasmid SCP1 and was kindly provided by D.A. Hopwood, Norwich, UK. Cultivation on plates (until spores developed) has been described earlier (Hopwood *et al.*, 1985; Koebsch *et al.*, 2009). Stock suspensions containing  $2.5 \times 10^9$  spores per ml of 40% glycerol were stored at  $-20^\circ\text{C}$ .

### Chemicals, dyes and enzymes

Chemicals for SDS gel electrophoresis were from Serva, and Sepharyl S-300 was from GE Healthcare Life Sciences. Other chemicals were purchased from Sigma. Trypsin was from Roche. The dyes propidium iodine and SYTO9 were purchased from Molecular probes.

### Test for the presence of prodigiosin and actinorhodin

A prodigiosin control was gained from cultures of *S. lividans*. Investigations for the presence of prodigiosin were performed as described earlier (Koebsch *et al.*, 2009). In addition, samples were tested by LC/MS for the presence of the characteristic molecular weight (393 Da) of prodigiosin. An analysis for the abundance of actinorhodin and its related compounds was performed as described earlier (Bystrykh *et al.*, 1996). Actinorhodin is red under acid and blue under alkaline conditions, and has an adsorption maximum at 640 nm (pH 11.5–14).

### Sucrose gradients

Samples of droplets were subjected to sedimentation or flotation in sucrose gradients as reported earlier (Siemieniowicz *et al.*, 2007). Samples (35  $\mu\text{l}$ ) were loaded onto a gradient (360  $\mu\text{l}$ ) if 30% to 5% sucrose (in 50 mM Tris/HCl, pH 7.4), which had been placed onto a cushion (50  $\mu\text{l}$ ) of 50% sucrose in 50 mM Tris/HCl, pH 7.4. Alternatively, the sample was adjusted to 40% sucrose, and overloaded with a gradient of 30% to 5% sucrose. Centrifugation was performed at 60,000 r.p.m. ( $\approx 132,000 g$ ) in the TLA 120.1 rotor of the Beckmann mini-ultracentrifuge for 60 min. Portions of 35  $\mu\text{l}$  were taken subsequently from the top to bottom.

### Analysis of proteins

A small portion (30  $\mu$ l) from droplets or fractions obtained after sedimentation was subjected to electrophoresis (12.5% SDS-PAGE). Each protein-containing band was carefully cut out individually. After in-gel digestion with trypsin, the generated peptides were separated by HPLC (reversed phase C18 column), and inline subjected to an ESI-ion source mass spectrometer (Bruker HCT). The archived data were compared with a protein databank (Swissport) via Mascot software package. The identified protein sequences were further analysed for their domains as well as the corresponding genes.

### Analyses of samples without treatment or after staining with fluorescent dyes

Portions of plates containing droplets (see Fig. 1A) were photographed (Canon Power Shot G2) using a macro lens (dioptr value of +4). Individual small droplets (on a plate, see Fig. 1B) were inspected with the Zeiss Axiovert microscope (Achromplan 4 $\times$ , NA 0.10) and photographed (Canon EOS 450D).

To visualize the life/dead status of hyphae, the dyes SYTO9 and propidium iodine are in use (Siemieniowicz and Schrempf, 2007). A mixture of propidium iodine and SYTO9 was prepared in Hepes as indicated by the manufacturer (Molecular probes) and injected directly ( $\sim$ 0.5  $\mu$ l) into the droplets. After incubation for 40 min, samples were analysed with the Laser scanning microscope (510 Meta/Zeiss) equipped with a Zeiss Plan Neofluar objective as described earlier. After excitation at 488 nm, detection of hyphae (green fluorescence, containing SYTO9 within DNA) followed at 500–530 nm (Meschke and Schrempf, 2010). Hyphae, which had taken up propidium iodine into their DNA, had a red fluorescence, which was detected in the presence of the LP 560 nm filter following excitation at 543 nm. Areas, which contained both types of hyphae, resulted in a merged (yellow) fluorescence (see Fig. 1C).

### Transmission electron microscopy

Samples of the droplets (5–10  $\mu$ l) were either used directly or pre-treated for 15 min with glutaraldehyde (0.25%). Samples were placed onto carbon-covered Cu or Ni grids (300 mesh, Plano). After removal of the excess of liquid, neutralized phosphotungstic acid (3% w/v) was added for 1 min. Then, the grids were rinsed on drops of distilled water (Hegermann *et al.*, 2006). Air-dried samples were analysed in a Zeiss EM 902A and imaged using a digitalized camera.

### Cryo-electron microscopy

Samples (5  $\mu$ l) were directly taken from droplets and applied to glow-discharged quantifoil copper grids (Plano; diameter of holes 2  $\mu$ m). A volume of 3.5  $\mu$ l of a suspension containing 10 nm gold clusters was added from the backside of the grid, blotted to remove water except for a thin film, and immediately plunged into liquid ethane ( $\approx$  -170°C) for embedding in vitreous ice for cryo-electron microscopy, essentially following the

procedure described in Hoffmann and colleagues (2008). Frozen grids were either stored in LN<sub>2</sub> or immediately inspected in a transmission electron microscope (Polaris G<sup>2</sup>; FEI, Eindhoven, the Netherlands), equipped with a field emission gun and a postcolumn energy filter (HR\_GIF or GIF 2000), at liquid nitrogen temperature. The microscopes were operated at 300 keV and a magnification of 41 000 $\times$ , corresponding to pixel sizes of 0.55 nm or 0.31 nm on the specimen level. Zero-loss images were recorded using 2048  $\times$  2048 postGIF CCD arrays (Gatan). Tilt series were taken between  $\pm$ 60° with 2° angle increments at -3.5 to -5  $\mu$ m defocus and a total dose of < 100 e<sup>-</sup>/Å<sup>2</sup>. The images were aligned by means of gold beads as fiducial markers. Three-dimensional reconstructions were calculated by weighted backprojection using the TOM toolbox (Nickell *et al.*, 2005). The data were binned once or processed in original resolution.

Statistical analyses of density distributions in tomograms of vesicles were performed as follows. Subareas of a number of z-slices from a particular structure (e.g. vesicle interior) from a three-dimensional data set were extracted and the common mean value and variance of voxel values calculated. The variances of four different tomogram areas (three vesicles and the background) were compared by means of the Bartlett test (homogeneity of variances). The result was highly significant ( $P < 0.001$ ), i.e. the variances could not be considered as statistically identical. Therefore, the data sets could not be investigated by means of variance analysis (ANOVA). As an alternative, histograms (separated into 10 bins) of voxel values from various equally sized subareas (60  $\times$  85 voxels, resulting in 5100 data points each) in the same z-slice were compared by the Chi-square test for homogeneity, assuming that the voxel values of all subareas follow the same distribution ( $H_0$  hypothesis).

### Acknowledgements

We thank Dagmar Müller for skilful technical assistance, Christian Hoffmann for valuable help during initial studies of cryo-electron microscopy and Dr Mathews Groves (EMBL, Hamburg) for kindly proofreading the manuscript.

### References

- Abdallah, A.M., Gey van Pittius, N.C., Champion, P.A., Cox, J., Luirink, J., Vandenbroucke-Grauls, C.M., *et al.* (2007) Type VII secretion – mycobacteria show the way. *Nat Rev Microbiol* **5**: 883–891.
- Aebersold, R., and Mann, M. (2003) Mass spectrometry-based proteomics. *Nature* **422**: 198–207.
- Akpe San Roman, S., Facey, P.D., Fernandez-Martinez, L., Rodriguez, C., Vallin, C., Del Sol, R., and Dyson, P. (2010) A heterodimer of EsxA and EsxB is involved in sporulation and is secreted by a type VII secretion system in *Streptomyces coelicolor*. *Microbiology* **156**: 1719–1729.
- August, P.R., Flickinger, M.C., and Sherman, D.H. (1994) Cloning and analysis of a locus (*mcr*) involved in mitomycin C resistance in *Streptomyces lavendulae*. *J Bacteriol* **176**: 4448–4454.
- Bendtsen, J.D., Jensen, L.J., Blom, N., Von Heijne, G., and Brunak, S. (2004) Feature-based prediction of non-classical and leaderless protein secretion. *Protein Eng Des Sel* **17**: 349–356.

- Bendtsen, J.D., Kiemer, L., Fausbøll, A., and Brunak, S. (2005) Non-classical protein secretion in bacteria. *BMC Microbiol* **5**: 58. doi:10.1186/1471-2180-5-58.
- Bonde, M.R., and McIntyre, G.A. (1968) Isolation and biology of a *Streptomyces* sp. causing potato scab in soils below pH 5.0. *Am J Potato Res* **45**: 273–278.
- Butler, M.J., Binnie, C., DiZonno, M.A., Krygsmann, P., Soltes, G.A., Soostmeyer, G., et al. (1995) Cloning and characterization of a gene encoding a secreted tripeptidyl aminopeptidase from *Streptomyces lividans* 66. *Appl Environ Microbiol* **61**: 3145–3150.
- Bystrykh, L.V., Fernández-Moreno, M.A., Herrema, J.K., Malpartida, F., Hopwood, D.A., and Dijkhuizen, L. (1996) Production of actinorhodin-related 'blue pigments' by *Streptomyces coelicolor* A3(2). *J Bacteriol* **178**: 2238–2244.
- Calderón, I.L., Arenas, F.A., Pérez, J.M., Fuentes, D.E., Araya, M.A., Saavedra, C.P., et al. (2006) Catalases are NAD(P)H-dependent tellurite reductases. *PLoS ONE* **1**: e70.
- Carrondo, M.A. (2003) Ferritins, iron uptake and storage from the bacterioferritin viewpoint. *EMBO J* **22**: 1959–1968.
- Castro, M.E., Molina, R., Díaz, W., Pichuantes, S.E., and Vásquez, C.C. (2008) The dihydrolipoamide dehydrogenase of *Aeromonas caviae* ST exhibits NADH-dependent tellurite reductase activity. *Biochem Biophys Res Commun* **375**: 91–94.
- Cayrol, C., Petit, C., Raynaud, B., Capdevielle, J., Guillemot, J.C., and Defais, M. (1995) Recovery of respiration following the SOS response of *Escherichia coli* requires RecA-mediated induction of 2-keto-4-hydroxyglutarate aldolase. *Proc Natl Acad Sci USA* **92**: 11806–11809.
- Chater, K.F., Biró, S., Lee, K.J., Palmer, T., and Schrempf, H. (2010) The complex extracellular biology of *Streptomyces*. *FEMS Microbiol Rev* **34**: 171–198.
- Chiang, S.K., Lou, Y.C., and Chen, C. (2008) NMR solution structure of KP-TerB, a tellurite-resistance protein from *Klebsiella pneumoniae*. *Cell Mol Life Sci* **67**: 179–199.
- Díaz, M., Esteban, A., Fernández-Abalos, J.M., and Santamaría, R.I. (2005) The high-affinity phosphate-binding protein PstS is accumulated under high fructose concentrations and mutation of the corresponding gene affects differentiation in *Streptomyces lividans*. *Microbiology* **151**: 2583–2592.
- Filloux, A. (2010) Secretion signal and protein targeting in bacteria: a biological puzzle. *J Bacteriol* **192**: 3847–3849.
- Frangakis, A.S., Böhm, J., Förster, F., Nickell, S., Nicastro, D., Typke, D., et al. (2002) Identification of macromolecular complexes in cryoelectron tomograms of phantom cells. *Proc Natl Acad Sci USA* **99**: 14153–14158.
- Golbik, R., Yu, C., Weyher-Stingl, E., Huber, R., Moroder, L., Budisa, N., and Schiene-Fischer, C. (2005) Peptidyl prolyl *cis/trans*-isomerases: comparative reactivities of cyclophilins, FK506-binding proteins, and parvulins with fluorinated oligopeptide and protein substrates. *Biochemistry* **44**: 16026–16034.
- Grillo, M.A., and Colombatto, S. (2004) Metabolism and function in animal tissues of agmatine, a biogenic amine formed from arginine. *Amino Acids* **26**: 3–8.
- Hegermann, J., Overbeck, J., and Schrempf, H. (2006) *In vivo* monitoring of the potassium channel KcsA in *Streptomyces lividans* hyphae using immuno-electron microscopy and energy-filtering transmission electron microscopy. *Microbiology* **152**: 2831–2841.
- Heo, G.Y., Kim, W.C., Joo, G.J., Kwak, Y.Y., Shin, J.H., Roh, D.H., et al. (2008) Deletion of *xylR* gene enhances expression of xylose isomerase in *Streptomyces lividans* TK24. *J Microbiol Biotechnol* **18**: 837–844.
- Hoffmann, C., Leis, A., Niederweis, M., Plitzko, J.M., and Engelhardt, H. (2008) Disclosure of the mycobacterial outer membrane: cryo-electron tomography and vitreous sections reveal the lipid bilayer structure. *Proc Natl Acad Sci USA* **105**: 3963–3967.
- Hopwood, D.A., Bibb, M.J., Chater, K.F., Kieser, T., Bruton, C.J., Kieser, H.M., et al. (1985) *Genetic Manipulation of Streptomyces: A Laboratory Manual*. Norwich, UK: John Innes Foundation.
- Imlay, J.A. (2008) Cellular defenses against superoxide and hydrogen peroxide. *Annu Rev Biochem* **77**: 755–776.
- Johnstone, D.B., and Waksman, S.A. (1947) Production of streptomycin by *Streptomyces bikiniensis*. *J Series Rutgers Uni* **55**: 317–236.
- Katan, M. (2005) New insights into the families of PLC enzymes: looking back and going forward. *Biochem J* **391**: e7–e9.
- Kempf, B., and Bremer, E. (1998) Uptake and synthesis of compatible solutes as microbial stress responses to high-osmolality environments. *Arch Microbiol* **170**: 319–330.
- Koebisch, I., Overbeck, J., Piepmeyer, S., Meschke, H., and Schrempf, H. (2009) A molecular key for building hyphae aggregates: the role of the newly identified *Streptomyces* protein HyaS. *Microb Biotechnol* **2**: 343–360.
- Kuehn, M.J., and Kesty, N.C. (2005) Bacterial outer membrane vesicles and the host–pathogen interaction. *Genes Dev* **19**: 2645–2655.
- Kulp, A., and Kuehn, M.J. (2010) Biological functions and biogenesis of secreted bacterial outer membrane vesicles. *Annu Rev Microbiol* **64**: 163–184.
- Kutzner, H.J. (1981) The family *Streptomycetaceae*. In *The Prokaryotes: A Handbook on Habitats, Isolation and Identification of Bacteria*. Starr, M.P., Stolp, H., Trüper, H.G., Balows, A., and Schlegel, H. (eds). Berlin, Germany: Springer-Verlag, pp. 2028–2090.
- Lee, E.Y., Choi, D.Y., Kim, D.K., Kim, J.W., Park, J.O., Kim, S., et al. (2009) Gram-positive bacteria produce membrane vesicles: proteomics-based characterization of *Staphylococcus aureus*-derived membrane vesicles. *Proteomics* **9**: 5425–5436.
- Li, Z., Clarke, A.J., and Beveridge, T.J. (1996) A major autolysin of *Pseudomonas aeruginosa*: subcellular distribution, potential role in cell growth and division and secretion in surface membrane vesicles. *J Bacteriol* **178**: 2479–2488.
- Martín, J.F., Casqueiro, J., and Liras, P. (2005) Secretion systems for secondary metabolites: how producer cells send out messages of intercellular communication. *Curr Opin Microbiol* **8**: 282–293.
- Mashburn-Warren, L.M., and Whiteley, M. (2006) Special delivery: vesicle trafficking in prokaryotes. *Mol Microbiol* **61**: 839–846.
- Meschke, H., and Schrempf, H. (2010) *Streptomyces lividans* inhibits the proliferation of the fungus *Verticillium dahliae*

- on seeds and roots of *Arabidopsis thaliana*. *Microb Biotechnol* **3**: 428–433.
- Nathan, C. (2004) The moving frontier in nitric oxide-dependent signaling. *Sci STKE* **257**: pe52.
- Nickell, S., Förster, F., Linaroudis, A., Net, W.D., Beck, F., Hegerl, R., *et al.* (2005) TOM software toolbox: acquisition and analysis for electron tomography. *J Struct Biol* **149**: 227–234.
- Niederweis, M., Danilchanka, O., Huff, J., Hoffmann, C., and Engelhardt, H. (2010) Mycobacterial outer membranes: in search of proteins. *Trends Microbiol* **18**: 109–116.
- Pan, Y.R., Lou, Y.C., Seven, A.B., Rizo, J., and Chen, C.J. (2011) NMR structure and calcium-binding properties of the tellurite resistance protein TerD from *Klebsiella pneumoniae*. *J Mol Biol* **405**: 1188–1201.
- Rudd, B.A., and Hopwood, D.A. (1979) Genetics of actinorhodin biosynthesis by *Streptomyces coelicolor* A3(2). *J Gen Microbiol* **114**: 35–43.
- Santos-Beneit, F., Rodríguez-García, A., Apel, A.K., and Martín, J.F. (2009) Phosphate and carbon source regulation of two PhoP-dependent glycerophosphodiester phosphodiesterase genes of *Streptomyces coelicolor*. *Microbiology* **155**: 1800–1811.
- Schaerlaekens, K., Schierová, M., Lammertyn, E., Geukens, N., Anné, J., and Van Mellaert, L. (2001) Twin-arginine translocation pathway in *Streptomyces lividans*. *J Bacteriol* **183**: 6727–6732.
- Schrempf, H. (2007) The family of Streptomycetaceae: part II molecular biology. In *The Prokaryotes*, Vol. **3**. Dworkin, M., Falkow, S., Rosenberg, E., Schleifer, K.H., and Stackebrandt, E. (eds). Berlin, Germany: Springer-Verlag, pp. 605–622.
- Sidhu, V.K., Vorhölter, F.J., Niehaus, K., and Watt, S.A. (2008) Analysis of outer membrane vesicle associated proteins isolated from the plant pathogenic bacterium *Xanthomonas campestris* pv. *campestris*. *BMC Microbiol* **8**: 87. doi:10.1186/1471-2180-8-87.
- Siemieniowicz, K.W., and Schrempf, H. (2007) Concerted responses between the chitin-binding protein secreting *Streptomyces olivaceoviridis* and *Aspergillus proliferans*. *Microbiology* **153**: 593–600.
- Siemieniowicz, K.W., Kajla, M.K., and Schrempf, H. (2007) Elucidating the biosynthesis of chitin filaments and their configuration with specific proteins and electron microscopy. *Macromol Biosci* **7**: 40–47.
- Stonehouse, M.J., Cota-Gomez, A., Parker, S.K., Martin, W.E., Hankin, J.A., Murphy, R.C., *et al.* (2002) A novel class of microbial phosphocholine-specific phospholipases C. *Mol Microbiol* **46**: 661–676.
- Williams, A.M., and McCoy, E. (1953) Degeneration and regeneration of *Streptomyces griseus*. *Appl Microbiol* **1**: 307–313.
- Yuan, J., Zweers, J.C., van Dijk, J.M., and Dalbey, R.E. (2010) Protein transport across and into cell membranes in bacteria and archaea. *Protein Sci* **17**: 785–789.